

ACOUSTIC LOCALIZATION OF RF CAVITY BREAKDOWN: STATUS AND PROGRESS*

P. Lane, P. Snopok^{†1}, Y. Torun¹, Illinois Institute of Technology, Chicago, USA
 A. Kochemirovskiy, University of Chicago, Chicago, USA
¹also at Fermi National Accelerator Laboratory, Batavia, USA

Abstract

Current designs for muon accelerators require high-gradient RF cavities to be placed in solenoidal magnetic fields. These fields help contain and efficiently reduce the phase space volume of source muons in order to create a usable muon beam for collider and neutrino experiments. It has been found that placing normal conducting RF cavities in strong magnetic fields reduces the threshold at which RF cavity breakdown occurs. To aid the effort to study RF cavity breakdown in magnetic fields, it would be helpful to have a diagnostic tool which can localize the source of breakdown sparks inside the cavity. These sparks generate thermal shocks to a small region of the inner cavity wall that can be detected and localized using microphones attached to the outer cavity surface. Presented here are the algorithms for and results from localizing simulated and experimental acoustic data from the Modular Cavity at the MuCool Test Area at Fermilab.

INTRODUCTION

To compliment current and future hadron colliders, higher energy lepton colliders will be needed to gain precision mass measurements of the Higgs and possible beyond-standard-model particles [1]. Using muons instead of electrons and positrons would allow collider designs that are not radiatively limited by synchrotron radiation energy losses. Also, neutrino factories employing muons could reduce systematic uncertainties in experiments studying beyond-standard-model physics through the observation of neutrino oscillations [2]. This is due to the fact that muons decay into a precise ratio of 50% muon and 50% electron [anti-]neutrinos.

The 2.2 μ s mean rest-frame lifetime of the muon necessitates that the muon bunch sizes be reduced quickly in order that enough time is allowed for the muon beam to be useful. The most promising technique for achieving beam sizes with acceptable phase space volumes is ionization cooling. This technique uses energy absorbers to reduce the phase space volume, and RF accelerating cavities to restore the energy lost in the absorbers [3]. To limit the muon beam size while the beam is cooled, strong solenoid magnets are employed.

Because muon ionization cooling channel designs will likely employ high-gradient, normal conducting RF cavities, the MuCool Test Area (MTA) group at Fermilab have been studying the behavior of such cavities in strong magnetic fields. It has been observed that the maximum accelerating gradient, or breakdown gradient, of a cavity subjected to

these conditions can be reduced. Breakdown results in the complete loss of the accelerating potential and electrical arcs, or “sparks”, that may cause damage to the cavity. Reducing the accelerating gradient of RF cavities in a cooling channel to prevent breakdown can increase the size and cost of the machine.

In order to improve the performance of accelerating cavities in strong magnetic fields, it would be useful to have a diagnostic tool that would indicate where breakdown sparks are occurring without having to shutdown the experiment and open the cavity to inspect damage. The following sections present an algorithm for locating the source of a breakdown spark thermal shock using data collected from eight microphones attached to the outside circular end plate surfaces of the Modular Cavity (MC). Furthermore, recent results of applying this algorithm to simulated and experimental acoustic data from the MC are also given.

ALGORITHM

A technique named Accumulated Correlation (AC) was chosen for the basis of the breakdown localization algorithm. It has been shown to be just as accurate as beamforming while being more computationally efficient like Time Difference of Arrival (TDOA) [4]. AC is a free-space localization technique, and as such assumes a non-dispersive medium where the only difference in signals at each microphone is the time at which they arrive. To compensate for the dispersive nature of the metal of the RF cavity walls, modifications were done to the base algorithm to improve its accuracy in the case of localizing a sound source on the opposite side of a metal RF cavity end plate.

Accumulated Correlation

AC starts by computing the cross-correlation between each pair of signals:

$$R_{ij}(\tau) = \int_{t'_0 - \frac{W}{2}}^{t'_0 + \frac{W}{2}} x_i(t)x_j(t - \tau)dt, \quad (1)$$

where τ is a particular delay value, t'_0 and W are the center and width of the time region in which the sound is expected to be heard, and x_i and x_j are the i th and j th microphone signals. Applying R_{ij} to a range of discrete values yields a cross-correlation vector. The value of each element in the vector gives an indication of how likely the corresponding delay, τ , is equal to the true delay between the two signals. The limits of integration determine the region in which the wavefront is expected to be.

* Work supported by Muon Accelerator Program

[†] psnopok@iit.edu

AC defines a set of M candidate source locations (i.e. a regular grid of test points), $\{\mathbf{q}_1, \mathbf{q}_2, \dots, \mathbf{q}_M\}$, and computes the difference of arrival times between each pair of transducers ($\tau_{ij, \mathbf{q}} = t_{j, \mathbf{q}} - t_{i, \mathbf{q}}$) for each candidate location \mathbf{q} . The cross-correlation vector elements corresponding to these time differences between signal pairs are summed to create an overall indication of how likely the sound originated from the candidate source location:

$$L_{AC}(\mathbf{q}) = \sum_{i=1}^N \sum_{j=i+1}^N R_{ij}(\tau_{ij, \mathbf{q}}). \quad (2)$$

The candidate source location with the largest corresponding sum is taken as the source location prediction [4].

Since propagation times are proportional to distances by a factor of the sound velocity, each time delay, $\tau = t_2 - t_1$, represents a physical half-hyperboloid of sound source positions for each pair of microphones. That is because a hyperbola can be defined as the set of points where the absolute value of the difference between the distances to those points from two stationary foci is constant:

$$|d_2 - d_1| = \tau v, \quad (3)$$

where $d_1 = t_1 v$, $d_2 = t_2 v$, and the microphones sit at the foci.

Therefore, in two dimensions AC can be visualized as the sum of a set of hyperbolic level curves. Each set of curves is associated with a particular pair of microphones, ij , and each level value is the value of the cross-correlation vector for ij , $R_{ij}(\tau)$, corresponding to a particular time delay τ . Figure 1 shows an example plot of these level curves for a particular ij (black crosses). Each 2D point is a particular \mathbf{q} , and the color at that point represents the value of the cross-correlation for the associated $\tau_{ij, \mathbf{q}}$.

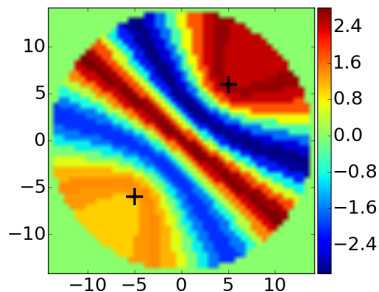


Figure 1: Example set of AC hyperbolic level curves for a microphone pair ij (black crosses). Each point is a candidate source location, \mathbf{q} , and its color is the cross-correlation value for the time delay between ij for that \mathbf{q} .

The sum over all sets of time delay level curves (one for each ij) can be seen in Fig. 2. The predicted source location is the point on this plot with the largest sum (darkest red).

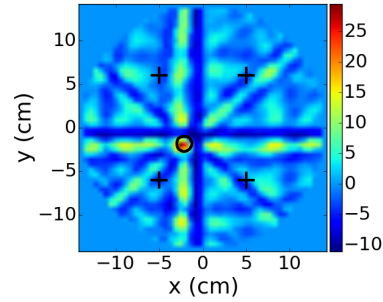


Figure 2: Example sums of all AC time delay level curves. The \mathbf{q} with the largest sum (darkest red) is the predicted source location. The actual source location is at the center of the black circle.

Octant Detection

An improvement to the algorithm resulted from constraining it to the general region in which the source was located. This was done by determining first the temporal order of the signals, and thus the order of the microphones by distance. Plugging this information into a binary decision tree produces the source octant. Figure 3 shows an example AC sums plot where more than one \mathbf{q} is highly likely, and the algorithm fails to make the correct choice. By restricting summation to only the source octant (region denoted by the white dashed lines), the \mathbf{q} closer to the true location is chosen as the prediction instead.

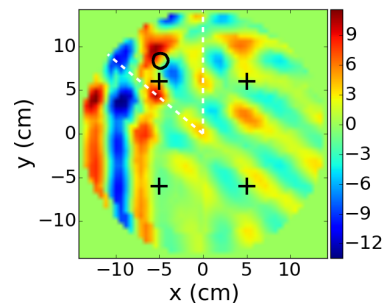


Figure 3: Example AC sums plot showing more than one highly-likely \mathbf{q} . The algorithm incorrectly predicts the \mathbf{q} near $(-5, 5)$ as the source location. By restricting summation to the octant denoted by the white line, the \mathbf{q} closer to the true location (black circle) is predicted, corresponding to the dark red spot near $(-5, 10)$.

Linear Scaling

Dispersion of acoustic waves in the metal end plate causes signal oscillations to get progressively wider with distance traveled. This has the effect of decreasing the effective sound speed as measured between the peaks of oscillations. To help compensate for this, the sound speed used in the AC

algorithm, v , was parameterized by two values with the unit of velocity, v_1 and v_2 , so that

$$v = v_1 + \frac{\Delta v}{1 \text{ cm}} r, \quad (4)$$

where $\Delta v = v_2 - v_1$, and r is the distance between the candidate source location and one of the microphones.

Using data from 100 simulated sparks with randomly chosen source locations, a parameter sweep of the two velocities was performed to optimize the values of v_1 and v_2 . The parameter sweep applied the localization algorithm while varying the values of v_1 and v_2 . It then calculated the residuals between the true source locations specified in the simulation and the predicted locations returned from the algorithm. The objective function for this optimization was the sum of the squares of the mean residuals and the standard deviation residuals.

The parameters that produced the smallest objective function value were $v_1 = 3.17 \times 10^5$ cm/s and $v_2 = 3.06 \times 10^5$ cm/s. As a reference, the shear and pressure wave speeds in copper (the material of the MC end plates) are 2.32×10^5 cm/s and 4.76×10^5 cm/s respectively. The plot of residuals for this parameterization is shown on the left in Fig. 4.

Another interesting set of parameters were those that minimized just the residuals mean. Specifically, these parameters were $v_1 = 3.01 \times 10^5$ cm/s and $v_2 = 2.10 \times 10^5$ cm/s. The right plot of Fig. 4 shows the residuals for this parameterization. Since the field in an RF accelerating cavity is generally highest near the beam axis, this parameterization is useful for producing more accurate predictions when the assumption is that the source of sparks will be within a radius of 6 cm from the beam axis.

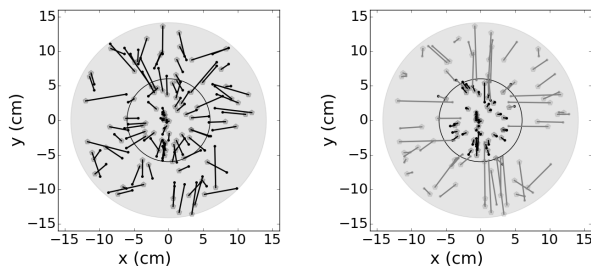


Figure 4: Reconstruction of the positions of 100 random, simulated sparks (pentagons) and their predictions (dots) for the two velocity parameterizations. Straight lines link predictions with true positions. The larger gray circle represents the MC end plate, while the smaller circle has a radius of 6 cm and is drawn to aid comparison of the two plots. The grayed out residuals in the right plot call attention to the improved accuracy of the predictions for source locations within a radius of 6 cm of the beam axis.

RESULTS

Simulation

Quantitatively, the mean and standard deviation of the simulation reconstruction residuals shown in the left plot of Fig. 4 are 2.6 cm and 1.5 cm respectively. This is sufficient for differentiating between sparks that occur near the beam axis and those that occur near the RF coupler (another high-field region).

For the residuals shown on the right in Fig. 4, both the mean and standard deviation are 2.2 cm. As was mentioned above, this second velocity parameterization is of primary importance when the spark sources are expected to be close to the beam axis. By including only those points whose true source location is within 6 cm of the beam axis, the mean and standard deviation of the residuals both become 0.7 cm.

Experiment

Two runs of the MC in a 3 T solenoidal magnetic field produced mirror-image damage pits on the upstream and downstream end plates in a region near the beam axis. These pits can be compared with spark source location predictions from the captured acoustic data. Though time did not allow a full analysis of the damage, pits produced during the first run had a standard deviation with respect to the pit centroid of 2.2 cm. Qualitatively this does not appear to have changed significantly following the second MC run. Furthermore, overlaying an image of the damage on both end plates with predictions shows general agreement in the distribution of pits and predictions. Figure 5 shows the upstream overlay. Red circles are the mapped pits from the first run. Green circles are the predictions for the second run. Predictions for the first run could not be produced due to a lack of data.

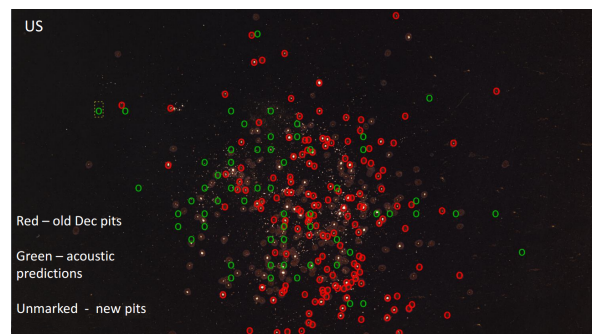


Figure 5: Overlay of damage pits and spark source location predictions from two 3T magnetic field runs of the MC.

CONCLUSION

Strong evidence suggests that RF cavity spark sources can be localized acoustically with an accuracy under 1 cm for sparks that occur within a radius of 6 cm of the beam axis. The accuracy is reduced to 2.6 cm if sparks occur at larger radii.

REFERENCES

- [1] C. Ankenbrandt *et al.*, “Status of muon collider research and development and future plans”, *Phys. Rev. ST Accel. Beams*, 2:081001, August 1999, doi:10.1103/PhysRevSTAB.2.081001.
- [2] S. Geer, “Neutrino beams from muon storage rings: characteristics and physics potential”, *Phys. Rev. D*, 57:6989–6997, June 1998, doi:10.1103/PhysRevD.57.6989.
- [3] R. Palmer, “Muon collider: introduction and status”, Feb. 1998, accessed 20 Apr. 2016, http://www.hep.princeton.edu/mumu/palmer/palmer_9802005.pdf
- [4] S. T. Birchfield, “A unifying framework for acoustic localization”, in *Proc. 12th European Signal Processing Conference*, Vienna, Austria, Sep. 2004, pp. 1127–1130.